

0017-9310(95)00012-7

# Development and investigation of three-phase model of the mushy zone for analysis of porosity formation in solidifying castings

A. V. KUZNETSOV

Mechanical Engineering Research Institute of Russian Academy of Sciences 101830 Moscow, Russia

and

K. VAFAI†

Department of Mechanical Engineering, The Ohio State University, Columbus, OH 43210, U.S.A.

(Received 27 July 1994 and in final form 12 December 1994)

**Abstract**—In this paper a three-phase model (liquid, solid and gas) of the mushy zone for investigation of porosity formation in solidifying castings is developed. This model takes into account the release of the dissolved gas from the alloy as well as heat transfer and interdendritic fluid flow in the mushy zone. An important aspect of this work is related to accounting for the term describing porosity formation in the continuity equation. The magnitude and influence of this term is estimated. Distributions of residual porosity in castings are calculated based on a uniform solidification assumption for the particular case of aluminum-rich Al–Cu castings. An analytical criterion, identifying conditions under which there will be no porosity formation, is established.

## 1. INTRODUCTION

An important task in modeling of casting processes is prediction of porosity distribution. This is because of the casting defects which are directly attributed to the porosity formation. One of the approaches used to predict porosity distribution is based on analyzing a number of parameters during the casting process (Piwonka and Flemings [1]; Davies [2]; Niyama *et al.* [3]; Pan *et al.* [4]; Hansen and Berry [5]). Viswanathan *et al.* [6] divided casting processes and alloy types into four groups, and suggested a different set of criteria functions for each group. Criteria functions are composed of thermal and solidification parameters such as temperature, fraction of solid, maximum thermal gradient at the end of freezing, isotherm velocity in the direction of the thermal gradient, instantaneous cooling rate, and local solidification time. These parameters are usually extracted from the numerical solutions. If computed local values of criteria functions are less than the critical value at a given position, presence of porosity at that position can be expected. Huang *et al.* [7] investigated sensitivity of criteria functions to thermal contact and phase change in solidification modeling.

Though this approach for some cases is proved to provide acceptable agreement with experimental data, it has some disadvantages. The main disadvantage is connected with the fact that porosity in this approach

is predicted not by solution of a physical problem but is based on some empirical correlations. Efforts to theoretically validate parameters governing porosity formation have been undertaken, for example, in Lecomte-Beckers [8] and Lee *et al.* [9]. In these publications interdendritic fluid flow for the two-phase region is considered and the criteria of porosity formation expressed in terms of solidification parameters are obtained from the fluid flow solution.

An alternative approach is based on direct analysis of coupled heat, mass, and fluid flow problem which arises from modeling of microprocesses in the mushy zone (Thevoz *et al.* [10]; Stefanescu *et al.* [11]). Kubo and Pehlke [12] suggested a model for shrinkage and gas porosity formation based on the assumption that the most important stage for creation of porosity defects is interdendritic feeding. Poirier *et al.* [13] considered formation of interdendritic porosity in aluminum-rich Al–Cu alloys. According to their model, interdendritic porosity arises in these alloys because solubility of hydrogen is less in the solid than in the liquid metal, so that some of the hydrogen is expelled into the interdendritic liquid.

Even though extensive studies of porosity formation are presented in recent publications, most of the models which are used for describing interdendritic fluid flow proceed from the assumption that porosity formation does not influence the flow. In other words, these models proceed from a two-phase model of the mushy zone (only liquid and solid) instead of a three-phase model (liquid, solid and gas).

†Author to whom correspondence should be addressed.

## NOMENCLATURE

$a$	thermal diffusivity, $\lambda/c_p\rho$ [ $\text{m}^2 \text{s}^{-1}$ ]	$q$	heat flux [ $\text{W m}^{-2}$ ]
$c_p$	specific heat at constant pressure [ $\text{J kg}^{-1} \text{K}^{-1}$ ]	$q_{\text{inf}}$	heat flux at the casting–chill interface [ $\text{W m}^{-2}$ ]
$C_{\text{eff}}$	effective specific heat per unit volume (with account for latent heat of fusion) [ $\text{J m}^{-3} \text{K}^{-1}$ ]	$r$	radius of pore [m]
$C_{\text{H0}}$	initial (melt) concentration of hydrogen in the alloy [weight %]	$R$	characteristic size of the casting [m]
$C_{\text{H}}^{\text{L}}$	concentration of dissolved hydrogen in liquid phase [weight %]	$S$	solubility of hydrogen [ $\text{cm}^3$ of $\text{H}_2$ per 100 g of alloy]
$C_{\text{H}}^{\text{S}}$	concentration of dissolved hydrogen in solid phase [weight %]	$S_c$	area of the casting which has a thermal contact with the chill [ $\text{m}^2$ ]
$\langle C_{\text{H}} \rangle$	average concentration of dissolved hydrogen in microvolume [weight %]	$t$	time [s]
$\langle C_{\text{H}}^* \rangle$	saturated average concentration of dissolved hydrogen in microvolume [weight %]	$\hat{t}$	duration of two-phase solidification [s]
$C_{\text{Cu0}}$	initial (melt) concentration of Cu in the alloy [weight %]	$T$	temperature [K]
$C_{\text{CuE}}$	concentration of Cu in liquid at eutectic temperature [weight %]	$v$	velocity [ $\text{m s}^{-1}$ ]
$C_{\text{Cu}}^{\text{L}}$	concentration of Cu in liquid phase [weight %]	$V_c$	volume of the casting [ $\text{m}^3$ ]
$C_{\text{Cu}}^{\text{S}}$	concentration of Cu in solid phase [weight %]	$x$	vertical coordinate [m]
$d$	base diameter of a dendrite arm (average size of the dendrite cell) [m]	$\bar{x}$	coordinate of position of pressure minimum in the casting at $t = \hat{t}$ [m].
$f_{\text{E}}$	weight fraction of eutectic	Greek symbols	
$f_{\text{L}}$	weight fraction of liquid	$\alpha$	heat transfer coefficient at the casting–chill interface [ $\text{W m}^{-2} \text{K}^{-1}$ ]
$f_{\text{S}}$	weight fraction of solid	$\beta$	metal volume shrinkage during solidification
$g$	gravitational acceleration [ $\text{m s}^{-2}$ ]	$\varepsilon$	volume fraction of porosity
$g_{\text{E}}$	volume fraction of eutectic	$\bar{\varepsilon}$	volume fraction of porosity calculated under the assumption that porosity formation does not influence the pressure distribution
$g_{\text{L}}$	volume fraction of liquid	$\delta$	dimensionless criteria of uniform solidification
$g_{\text{S}}$	volume fraction of solid	$\lambda$	thermal conductivity of the alloy [ $\text{W m}^{-1} \text{K}^{-1}$ ]
$\text{H}_2(\text{g})$	gaseous hydrogen	$\mu$	absolute viscosity [ $\text{kg m}^{-1} \text{s}^{-1}$ ]
$H$	hydrogen dissolved in liquid phase	$\rho$	density [ $\text{kg m}^{-3}$ ]
$k_{\text{H}}$	solute distribution coefficient for hydrogen	$\bar{\rho}$	average density [ $\text{kg m}^{-3}$ ].
$k_{\text{Cu}}$	solute distribution coefficient for copper	Subscripts	
$\Delta h$	latent heat of fusion [ $\text{J kg}^{-1}$ ]	c	casting
$K$	permeability [ $\text{m}^2$ ]	ch	chill
$K_{\text{eq}}$	equilibrium constant [ $\text{Pa}^{-1/2}$ ]	E	eutectic
$L$	length of the casting in vertical direction [m]	g	gas phase
$M_{\text{S}}$	volumetric specific surface area of a typical dendrite arm [ $\text{m}^{-1}$ ]	L	liquid phase
$P$	pressure in the mushy zone [Pa]	max	maximum value
$\bar{P}$	pressure in the mushy zone calculated under the assumption that porosity formation does not influence the pressure distribution [Pa]	min	minimum value
$P_{\text{atm}}$	atmospheric pressure [Pa]	S	solid phase
$P_{\text{g}}$	pressure in the gas phase [Pa]	0	initial.
		Other symbols	
		$\langle \Phi \rangle$	$= 1/V \int_{V_{\Psi}} \Phi dV$ , local volume average of a quantity $\Phi$
		$\langle \Phi \rangle^{\Psi}$	$= 1/V_{\Psi} \int_{V_{\Psi}} \Phi dV$ , intrinsic local volume average of a quantity $\Phi$ associated with phase $\Psi$
		$\theta(\xi)$	$= \begin{cases} 0 & \xi < 0 \\ 1 & \xi \geq 0 \end{cases}$

Investigation of influence porosity formation on heat and mass transfer processes in the mushy zone is of importance because nucleation and growth of porosity are important physical phenomena occurring in the mushy zone and accuracy of porosity prediction surely depends on their accounting.

Derivation of the set of governing equations for the mushy zone based on mixture theory approach is reported in Bennon and Incropera [14] and Prescott *et al.* [15]. Derivation of the set of governing equations based on volume-averaging procedure is presented in Ganesan and Poirier [16] and in Ni and Beckermann [17]. Numerical modeling of solidification of alloys based on these set of equations is reported in Beckermann and Viskanta [18], Felicelli *et al.* [19, 20].

The present investigation proceeds from the set of governing equations obtained by the volume averaging technique. To take into account the influence of porosity formation, a three-phase model of the mushy zone is developed. For this purpose, distinguished from previous investigations, a continuity equation which accounts for porosity growth is suggested. The particular form of this equation is developed based on thermodynamic relationships for aluminum-rich Al-Cu alloys. Equations of the mathematical model are solved assuming uniform solidification. Distributions of residual porosity in castings for this case are obtained.

## 2. PROBLEM STATEMENT AND ANALYSIS

### 2.1. Governing equations

In the present investigation Darcy's law will be utilized within the mushy zone. Darcy's law has frequently been used to model the flow in a dendritic mushy zone (Mehrabian *et al.* [21]; Sreat and Weinberg [22]; Fujii *et al.* [23]; Ridder *et al.* [24]; Maples and Poirier [25]). Ganesan and Poirier [16] showed that the Darcy's law is valid when the flow is slow and steady, the volume fraction of liquid is uniform and constant, and liquid-liquid interactions are negligibly small.

Equiaxial dendritic structure of the mushy zone is assumed. Assuming that Darcy's law can be used as a momentum equation for interdendritic fluid flow in the mushy zone, the set of equations governing the flow in the mushy zone is put in the following form

#### 2.1.1. Momentum equation.

$$\mathbf{v} = -\frac{K}{\mu}(\nabla P - \rho_L \mathbf{g}) \quad (1)$$

where  $\mathbf{v} = \langle \mathbf{v}_L \rangle$ ,  $P = \langle P_L \rangle^L$ . Poirier [26] recommends to use the Blake-Kozeny model for permeability when it is necessary to extrapolate beyond the scope of experimental results. Following Beckermann and Viskanta [18] and Ampuero *et al.* [27] the following expression for permeability of the mushy zone is utilized

$$K = \frac{g_L^3}{5M_s^2(1-g_L)^2} \quad (2)$$

where volumetric specific surface area of a typical dendrite arm is approximated as  $M_s \approx 6/d$ .

Using equation (2), momentum equation (1) can be written as

$$\mathbf{v} = -\frac{g_L^3}{5\mu M_s^2(1-g_L)^2}(\nabla P - \rho_L \mathbf{g}). \quad (3)$$

2.1.2. Mass conservation equation (assuming that the gas and solid velocities are negligible).

$$\frac{\partial}{\partial t}(\rho_s g_s + \rho_L g_L + \rho_g \varepsilon) + \nabla \cdot \rho_L \mathbf{v} = 0 \quad (4)$$

where

$$g_s + g_l + \varepsilon = 1. \quad (5)$$

It should be noted that permeability of the mushy zone is an uncertain part of modeling of the processes in the two-phase region. In this work the Blake-Kozeny model is used for permeability when it is necessary to extrapolate beyond the scope of the experimental results. Generally, the Blake-Kozeny model is considered to be reliable expression. However, considering the permeability of the three-phase mixture would be physically the most correct approach. Unfortunately, there are no experimental results available for such an approach for the mushy zone. Therefore, to avoid introducing additional errors in the numerical calculations, the more traditional Blake-Kozeny model was adopted.

Density of gas is negligibly small compared to densities of solid and liquid phases, therefore equation (4) can be recast as

$$\frac{\partial}{\partial t}[\rho_s g_s + \rho_L(1-g_s-\varepsilon)] + \nabla \cdot \rho_L \mathbf{v} = 0.$$

Assuming that densities of solid and fluid phases do not depend on time, this equation can be put in the following form

$$\beta \frac{\partial g_s}{\partial t} - \frac{\partial \varepsilon}{\partial t} + \nabla \cdot \mathbf{v} = 0 \quad (6)$$

where  $\beta = (\rho_s - \rho_L)/\rho_L$  (volume shrinkage during solidification).

In the present analysis, we consider one-dimensional filtration of interdendritic fluid (only in the vertical direction). For this case, substitution of equation (3) in equation (6) results in

$$\beta \frac{\partial g_s}{\partial t} - \frac{\partial \varepsilon}{\partial t} = \frac{1}{5\mu M_s^2} \frac{\partial}{\partial x} \left\{ \frac{g_L^3}{[1-g_L]^2} \left( \frac{\partial P}{\partial x} - \rho_L g \right) \right\}. \quad (7)$$

Weight fractions of liquid and solid are connected by the following relationship when the density of the gas phase is neglected

$$f_L + f_s = 1. \quad (8)$$

Using equation (8) along with equation (5), it is easy to show that

$$\begin{aligned} g_L &\approx f_L(1-\varepsilon) \\ g_S &\approx f_S(1-\varepsilon). \end{aligned} \quad (9)$$

Using the above result in equation (7) yields

$$\begin{aligned} \beta \frac{\partial f_S}{\partial t} (1-\varepsilon) - \frac{\partial \varepsilon}{\partial t} (1 + \beta f_S) \\ = \frac{1}{5\mu M_S^2} \frac{\partial}{\partial x} \left\{ \frac{(1-\varepsilon)^3 (1-f_S)^3}{[1-(1-\varepsilon)(1-f_S)]^2} \left( \frac{\partial P}{\partial x} - \rho_L g \right) \right\}. \end{aligned} \quad (10)$$

Equations (4), (6), (7) and (10) are different forms of the mass conservation equation which takes into account influence of not only solidification, but also of porosity formation processes on interdendritic fluid flow in the mushy zone.

Considering that  $\varepsilon$  and  $\beta$  are small parameters, some of the terms in equation (10) are neglected in the first approximation. The final form of equation (10) is

$$\beta \frac{\partial f_S}{\partial t} - \frac{\partial \varepsilon}{\partial t} = \frac{1}{5\mu M_S^2} \frac{\partial}{\partial x} \left\{ \frac{(1-f_S)^3}{f_S^2} \left( \frac{\partial P}{\partial x} - \rho_L g \right) \right\}. \quad (11)$$

It should be noted that nucleation of voids is an important and interesting physical phenomenon, which requires a separate consideration. However, in this work our main focus is the three-phase model, and we have avoided inclusion of nucleation phenomenon assuming that there are enough nucleation centers and there is no hindrance for formation of porosity.

## 2.2. Determination of the rate of porosity formation

Equation (3) and one of equations (4), (6), (7), (10) or (11) describe a three-phase model of the mushy zone (because they account for liquid, solid and gas phases). To obtain an equation for the second term in the right-hand side of the continuity equation, it is necessary to use thermodynamic relationships describing porosity formation for the particular alloy. In the present investigations, thermodynamic relationships for Al-rich Al-Cu alloys are utilized.

To obtain an equation for  $\partial \varepsilon / \partial t$  for this particular case, the thermodynamic approach to porosity prediction presented in Poirier *et al.* [13] is utilized. According to their investigation it is necessary to consider only hydrogen as a contributor to microporosity because it is the only gas with measurable solubility

pressure of hydrogen in the gas phase via the equilibrium relationship. Concentration of the dissolved hydrogen in liquid phase can be calculated utilizing the equilibrium constant from the reaction equation  $\frac{1}{2} \text{H}_2(\text{g}) = \underline{\text{H}}$

$$K_{\text{eq}} = \frac{C_{\text{H}}^{\text{L}}}{P_{\text{g}}^{1/2}} \quad (12)$$

where  $K_{\text{eq}}$  can be expressed in terms of hydrogen solubility  $K_{\text{eq}} = K_0 S$  and  $K_0 = 2.822 \times 10^{-7}$ .

According to the experimental data presented in Opie and Grant [28], who put their results in the form of van't Hoff equation, solubility of hydrogen in Al-Cu liquid alloys can be determined as

$$\ln S = -A/T + B \quad (13)$$

where  $S$  is the solubility, in  $\text{cm}^3$  of  $\text{H}_2(\text{g})$  per 100 g alloy, in equilibrium with 1 atm pressure of  $\text{H}_2(\text{g})$ , and functions  $A$  and  $B$  are determined by concentration of copper in the Al-Cu alloy:

$$A = a_0 + a_1 (C_{\text{Cu}}^{\text{L}})^{1/2} - a_2 C_{\text{Cu}}^{\text{L}} + a_3 (C_{\text{Cu}}^{\text{L}})^{3/2} \quad (14a)$$

$$B = b_0 + b_1 (C_{\text{Cu}}^{\text{L}})^{1/2} - b_2 C_{\text{Cu}}^{\text{L}} + b_3 (C_{\text{Cu}}^{\text{L}})^{3/2} \quad (14b)$$

where  $a_0 = 5871$ ,  $a_1 = 826.4$ ,  $a_2 = 125.4$ ,  $a_3 = 1.437$ ;  $b_0 = 6.033$ ,  $b_1 = 0.7007$ ,  $b_2 = 0.1859$ ,  $b_3 = 0.01032$  and  $C_{\text{Cu}}^{\text{L}}$  is the weight concentration of copper in liquid phase.

The solute equation for the case when macrosegregation is absent (it is our case because we assume uniform solidification) is considered in Rappaz and Voller [29]. They showed that, assuming rapid diffusion within the liquid phase (locally uniform concentration within the liquid phase) and no solute back diffusion within the solid phase, the concentration of solute (copper) in interdendritic liquid is described by the so-called Scheil equation

$$C_{\text{Cu}}^{\text{L}} = C_{\text{Cu}0} (1-f_S)^{(k_{\text{Cu}}-1)}. \quad (15)$$

According to Poirier *et al.* [13]  $k_{\text{Cu}} = 0.173$  in the above equation.

The dependence  $C_{\text{H}}^{\text{L}} = C_{\text{H}}^{\text{L}}(f_S, T)$  can be now found from equations (12)–(15). First equation (12) can be written as

$$C_{\text{H}}^{\text{L}} = K_0 S(f_S, T) P_{\text{g}}^{1/2}. \quad (16)$$

Next using equations (14) and (15) in equation (13), will result in eqn (17):

$$\begin{aligned} S(f_S, T) = \exp \left\{ - \frac{a_0 + a_1 [C_{\text{Cu}0} (1-f_S)^{(k_{\text{Cu}}-1)}]^{1/2} - a_2 C_{\text{Cu}0} (1-f_S)^{(k_{\text{Cu}}-1)} + a_3 [C_{\text{Cu}0} (1-f_S)^{(k_{\text{Cu}}-1)}]^{3/2}}{T} \right\} \\ \times \exp \{ b_0 + b_1 [C_{\text{Cu}0} (1-f_S)^{(k_{\text{Cu}}-1)}]^{1/2} - b_2 C_{\text{Cu}0} (1-f_S)^{(k_{\text{Cu}}-1)} + b_3 [C_{\text{Cu}0} (1-f_S)^{(k_{\text{Cu}}-1)}]^{3/2} \}. \end{aligned} \quad (17)$$

in aluminium. It is assumed that concentration of the dissolved hydrogen in metal is connected with

On the other hand, assuming rapid diffusion of dissolved hydrogen both in liquid and solid within the

microvolume, its concentration in interdendritic liquid can be calculated according to the Lever rule [13]:

$$C_H^L = \frac{\langle C_H \rangle}{(1-f_s) + k_H f_s} \quad (18)$$

where  $k_H = 0.069$ .

Equating expressions (16) and (18), the following equation for average concentration of hydrogen in microvolume is obtained

$$\langle C_H \rangle = K_0 S(f_s, T) P_g^{1/2} [(1-f_s) + k_H f_s] \quad (19)$$

where the function  $S(f_s, T)$  is determined by equation (17).

Equation (19) determines average concentration of hydrogen in microvolume in the region where porosity forms. In the region where there is no porosity the average hydrogen concentration still equals the initial (melt) hydrogen concentration in the alloy

$$\langle C_H \rangle = C_{H_0}$$

To obtain the equation for saturated concentration of dissolved hydrogen,  $\langle C_H^* \rangle$ , in microvolume corresponding to some particular value of pressure,  $P$ , in the mushy zone, it is necessary to use  $P$  instead of  $P_g$  in equation (19)

$$\langle C_H^* \rangle = K_0 S(f_s, T) P^{1/2} [(1-f_s) + k_H f_s]. \quad (20)$$

To obtain the equation for the rate of porosity formation it is necessary to make reasonable assumptions concerning conditions when porosity arises in the mushy zone. Usually it is assumed [12, 13] that a gas pore is stable when the pressure in the gas phase is large enough to overcome the pressure of liquid metal within the mushy zone plus the surface tension when the gas phase has a radius small enough to fit in the inter-crystal (interdendritic) space

$$P_g \geq P + \frac{2\sigma}{r}. \quad (21)$$

In ref. [12] it is suggested that diameter of the pore is the same as the dendrite cell size, and to estimate the dendrite cell size the following correlation is utilized

$$d = b \Delta \theta_f^n \quad (22)$$

where  $\Delta \theta_f$  is the local solidification time, and  $b$  and  $n$  are positive constants.

For the uniform solidification the temperature variation within the casting is small compared to the interval of solidification. Therefore, local solidification

time must be relatively large and the same for all points of the casting (only in this case temperature gradients within the casting can be neglected). Consequently, from equation (22) it follows that dendrite cell size for uniform solidification will be considerably larger than for directional solidification considered in ref. [13]. Therefore the second term on the right-hand side of equation (21) is neglected in the present analysis.

For this case from equation (21) it follows that porosity will arise when pressure in the mushy zone becomes less than pressure in the gas phase. In other words, porosity arises when saturated average concentration of hydrogen in microvolume becomes less than the initial (melt) concentration  $C_{H_0}$  (that is when the hydrogen gas can no longer be dissolved in the mushy zone)

$$\langle C_H^* \rangle \leq C_{H_0}$$

Using equation (20) this condition can be put in the following form

$$C_{H_0} - K_0 S(f_s, T) P^{1/2} [(1-f_s) + k_H f_s] \geq 0. \quad (23)$$

We assume that there is no macroliquation of hydrogen, therefore decrease of dissolved hydrogen concentration leads to gas phase formation. Using equation (23) the mass rate of gas phase formation can be found as

$$\frac{\partial m_{H_2}}{\partial t} = - \frac{1}{100} \frac{\partial \langle C_H \rangle}{\partial t} \times \theta (C_{H_0} - K_0 S(f_s, T) P^{1/2} [(1-f_s) + k_H f_s]) \quad (24)$$

where  $m_{H_2}$  is mass of the gas phase per 1 kg of alloy and

$$\theta(\xi) = \begin{cases} 0 & \xi < 0 \\ 1 & \xi \geq 0 \end{cases}$$

According to ideal gas equation of state the rate of change of the volume of the gas phase per 1 kg of alloy can be written as

$$\frac{\partial V_{H_2}}{\partial t} = \frac{\tilde{R}T}{M_{H_2} P} \frac{\partial m_{H_2}}{\partial t}. \quad (25)$$

The rate of porosity growth can be found now from equations (20), (24), (25) as

$$\frac{\partial \varepsilon}{\partial t} = \frac{1}{V_{H_2} + V_s + V_L} \frac{\partial V_{H_2}}{\partial t} = - \frac{\theta (C_{H_0} - K_0 S(f_s, T) P^{1/2} [1 - f_s (1 - k_H)])}{\frac{\tilde{R}T}{M_{H_2} P} [C_{H_0} - K_0 S(f_s, T) P^{1/2} [1 - f_s (1 - k_H)]] + 100 \left( \frac{f_s}{\rho_s} + \frac{1 - f_s}{\rho_L} \right)} \times \frac{\tilde{R}T}{M_{H_2} P} K_0 \times \left\{ \frac{\partial S(f_s, T)}{\partial t} P^{1/2} [1 - f_s (1 - k_H)] + \frac{\partial P^{1/2}}{\partial t} S(f_s, T) [1 - f_s (1 - k_H)] - S(f_s, T) P^{1/2} (1 - k_H) \frac{\partial f_s}{\partial t} \right\}. \quad (26)$$

Substitution of equation (26) into equation (11) leads to the following equation for pressure in the mushy zone

$$\frac{\Delta T_c}{T_L - T_s} = \frac{\alpha R}{\lambda} \frac{T_c - T_{ch}}{T_L - T_s} = \delta. \quad (31)$$

$$\begin{aligned} \beta \frac{\partial f_s}{\partial t} + \frac{\theta(C_{H_0} - K_0 S(f_s, T) P^{1/2} [1 - f_s(1 - k_H)])}{M_{H_2} P [C_{H_0} - K_0 S(f_s, T) P^{1/2} [1 - f_s(1 - k_H)]] + 100 \left( \frac{f_s}{\rho_s} + \frac{1 - f_s}{\rho_L} \right) M_{H_2} P K_0} \frac{\bar{R}T}{M_{H_2} P} K_0 \\ \times \left\{ \frac{\partial S(f_s, T)}{\partial t} P^{1/2} [1 - f_s(1 - k_H)] + \frac{1}{2P^{1/2}} \frac{\partial P}{\partial t} S(f_s, T) [1 - f_s(1 - k_H)] - S(f_s, T) P^{1/2} (1 - k_H) \frac{\partial f_s}{\partial t} \right\} \\ = \frac{1}{5\mu M_s^2} \frac{\partial}{\partial x} \left\{ \frac{(1 - f_s)^3}{f_s^2} \left( \frac{\partial P}{\partial x} - \rho_L g \right) \right\}. \quad (27) \end{aligned}$$

A scheme of solidifying casting and of pressure distribution in it is depicted in Fig. 1. Boundary and initial conditions for equation (27) are:

$$x = 0 \quad P = P_{atm} \quad (28a)$$

$$x = L \quad \frac{\partial P}{\partial x} = \rho_L g \quad (28b)$$

$$t = 0 \quad P = P_{atm} + \rho_L g x. \quad (28c)$$

Equation (28b) is obtained from equation (3) taking into account absence of interdendritic fluid flow at the bottom of the casting.

After pressure distribution is determined, porosity distribution in the mushy zone can be calculated from the following equation:

$$\begin{aligned} \varepsilon = \frac{V_{H_2}}{V_{H_2} + V_s + V_L} \\ = \frac{\frac{\bar{R}T}{M_{H_2} P} [C_{H_0} - K_0 S(f_s, T) P^{1/2} [1 - f_s(1 - k_H)]] \theta(C_{H_0} - K_0 S(f_s, T) P^{1/2} [1 - f_s(1 - k_H)])}{\frac{\bar{R}T}{M_{H_2} P} [C_{H_0} - K_0 S(f_s, T) P^{1/2} [1 - f_s(1 - k_H)]] + 100 \left( \frac{f_s}{\rho_s} + \frac{f_L}{\rho_L} \right)}. \quad (29) \end{aligned}$$

### 2.3. Solution of solidification problem

For many practical cases temperature variation within the solidifying casing is considerably less than the interval of solidification. Temperature variation within the casting can be estimated as

$$\Delta T_c \approx \frac{q_{inf} R}{\lambda} = \frac{\alpha(T_c - T_{ch}) R}{\lambda} \quad (30)$$

where  $q_{inf}$  is the heat flux at the casting–chill interface,  $\lambda$  is the thermal conductivity of the alloy, and  $R$  is the characteristic size of the casting.

From equation (30) it follows that

Thus if  $\delta \ll 1$ , then the temperature variation within the solidifying casting is considerably less than the interval of solidification. We consider only this case and assume that temperature variation within the casting can be neglected.

The most recent investigations of heat transfer coefficient at the casting–mold interface are reported in refs. [30, 31]. Heat transfer coefficient depends on the magnitude of interface gap due to the thermal contraction of cast metal as it solidifies. However, in this investigation we follow the research by Berry [32] and assume a constant value of gap width. This approximation leads to a constant value of the interfacial heat transfer coefficient. Additionally a constant temperature of the chill is assumed.

According to Al–Cu phase diagram (Murray [33]) during solidification of aluminum-rich Al–Cu alloy

concentration of copper in liquid phase increases until it reaches the eutectic composition ( $C_{CuE} = 32.7$  weight %). After the eutectic composition is reached, the rest of the liquid phase solidifies at constant temperature  $T_E$ . Amount of eutectic in alloy can be calculated according to equation (15):

$$f_E^{k_{Cu}-1} = \frac{C_{CuE}}{C_{Cu0}}. \quad (32)$$

From equation (32) it follows that for the alloy with  $C_{Cu0} = 4.5$  weight % the amount of eutectic is  $f_E = 0.09088$ . Thus there are two stages of solidification process. At the first stage alloy solidifies within the temperature range  $T_L(f_L) - T_E$ , at the

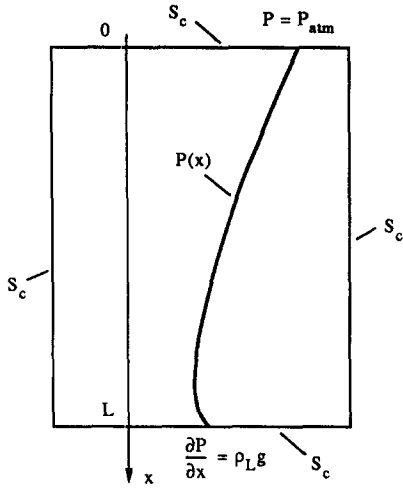


Fig. 1. Schematic of the solidifying casting.

second stage, which begins when  $f_L = f_E$ , the alloy solidifies at constant temperature  $T_E$ . It is assumed that the second stage does not influence the porosity distribution in the casting, therefore we must calculate porosity formation only during the first stage.

In addition it is assumed that interdendritic fluid flow does not significantly influence the heat transfer processes in the casting. Under the assumptions discussed above the energy equation for the casting process can be put into the following form (using the enthalpy approach):

$$V_c \left[ \frac{\Delta h(1-f_E)}{T_L - T_E} + \bar{c}_p \right] \bar{\rho} \frac{\partial T}{\partial t} = -\alpha(T - T_{ch})S_c \quad (33)$$

where  $V_c$  is the volume of the casting,  $S_c$  is the area of the casting which has a thermal contact with the chill (Fig. 1),  $\bar{\rho} = \rho_L + \rho_E/2$ ,  $\bar{c}_p = (c_p)_L + (c_p)_E/2$ .

Solution of the equation (33) with initial conditions  $T|_{t=0} = T_L$  (cooling of the metal from temperature of pouring to  $T_L$  is not considered because in our model this period does not influence the porosity formation) is

$$T = T_{ch} + (T_L - T_{ch}) \exp(-\Omega t) \quad (34)$$

$$\text{where } \Omega = \frac{S_c \alpha}{V_c \left[ \frac{\Delta h(1-f_E)}{T_L - T_E} + \bar{c}_p \right] \bar{\rho}}$$

$$\bar{\varepsilon}(x, \hat{t}) = \frac{\bar{R}T}{M_{H_2}P} [C_{H_0} - K_0 S(1-f_E, T_E) \bar{P}^{1/2}(x, \hat{t}) [1 - (1-f_E)(1-k_H)]]$$

$$\times \frac{\theta(C_{H_0} - K_0 S(1-f_E, T_E) \bar{P}^{1/2}(x, \hat{t}) [1 - (1-f_E)(1-k_H)])}{M_{H_2}P [C_{H_0} - K_0 S(1-f_E, T_E) \bar{P}^{1/2}(x, \hat{t}) [1 - (1-f_E)(1-k_H)]] + 100 \left( \frac{1-f_E}{\rho_s} + \frac{f_E}{\rho_L} \right)} \quad (37)$$

The first stage of solidification ends as soon as  $T = T_E$ , consequently the time which signifies the end of this stage can be calculated as

$$\hat{t} = \frac{1}{\Omega} \ln \left[ \frac{T_L - T_{ch}}{T_E - T_{ch}} \right]$$

Assuming that weight fraction of the solid phase is linearly connected with the temperature of metal in the mushy zone

$$f_s = (1-f_E) \frac{T_L - T}{T_L - T_E}$$

the equation for the volume fraction of solid can be obtained from equation (34) as

$$f_s = (1-f_E) \frac{T_L - T_{ch}}{T_L - T_E} [1 - \exp(-\Omega t)] \quad (35)$$

It should be noted that the entire analysis presented in this work is based on the assumption that non-Darcian effects are negligible and that the local thermal equilibrium prevails. As shown in refs. [34-39] these effects can introduce significant errors in the predictions.

### 3. SOLUTION

#### 3.1. Analytical solution of porosity formation problem for the simplified case

A simplified analytical solution of equation (27) with boundary conditions (28a) and (28b) can be obtained under the assumption that porosity formation does not influence the pressure distribution. It is exactly the same assumption which was adopted by Poirier *et al.* [13] in analyzing porosity formation problem. Under this assumption the second term on the left-hand side of equation (27) can be neglected and the pressure distribution is

$$\bar{P} = P_{atm} + \rho_L g x - \beta \frac{5\mu M_s^2 f_s^2}{(1-f_s)^3} \frac{\partial f_s}{\partial t} \left( Lx - \frac{x^2}{2} \right) \quad (36)$$

where the function  $f_s(t)$  is determined by equation (35).

According to equation (29) porosity distribution in casting after the end of two-phase solidification (when  $f_s = f_E$ ) can be calculated from the following equation:

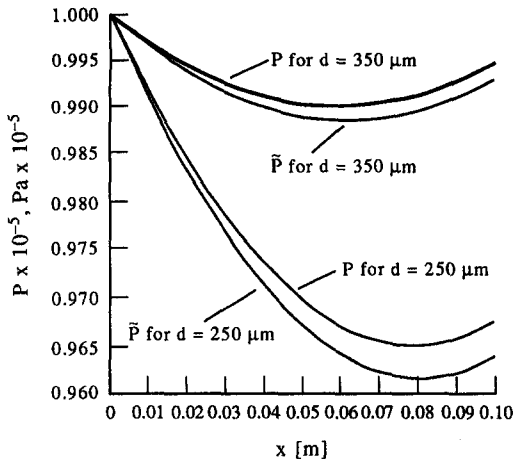


Fig. 2. Comparison of the numerical solution  $P$  of equation (38) and analytical solution  $\bar{P}$  given by equation (36) for different values of dendrite cell size  $d$ .

Equation (37) determines distribution of residual porosity in the casting under the assumption that the porosity distribution does not influence the pressure distributions.

3.2. Numerical steady-state solution of porosity formation problem

Since the change of the pressure in the mushy zone is slow, the non-stationary term  $\partial P/\partial t$  in equation (27) can be neglected (the influence of this term is estimated later on) and pressure distribution can be calculated from the following steady-state equation

$$\beta \frac{\partial f_s}{\partial t} + \frac{\theta(C_{H_0} - K_0 S(f_s, T) P^{1/2} [1 - f_s(1 - k_H)])}{M_{H_2} P [C_{H_0} - K_0 S(f_s, T) P^{1/2} [1 - f_s(1 - k_H)] + 100 \left( \frac{f_s}{\rho_s} + \frac{1 - f_s}{\rho_L} \right) M_{H_2} P K_0} \frac{\bar{R}T}{M_{H_2} P} K_0 \times$$

$$\left\{ \frac{\partial S(f_s, T)}{\partial t} P^{1/2} [1 - f_s(1 - k_H)] - S(f_s, T) P^{1/2} (1 - k_H) \frac{\partial f_s}{\partial t} \right\} = \frac{1}{5\mu M_s^2} \frac{\partial}{\partial x} \left\{ \frac{(1 - f_s)^3}{f_s^2} \left( \frac{\partial P}{\partial x} - \rho_L g \right) \right\}. \quad (38)$$

The function  $S(f_s, T)$  in equation (38) is determined by equation (17) and the transient temperature distribution,  $T(t)$  and the weight fraction of the solid  $f_s(t)$  are determined by equations (34) and (35), respectively.

To calculate residual porosity distribution  $\varepsilon(x, \hat{t})$  without the assumption that porosity formation does not influence pressure distribution in the mushy zone, it is necessary to use equation (37) utilizing the numerical solution  $P(x, \hat{t})$  of equation (38) instead of the analytical solution  $\bar{P}(x, \hat{t})$ .

Comparison of the numerical solution of equation (38) with boundary conditions (28a) and (28b) and the analytical solution (36) for different values of dendrite cell size is depicted in Fig. 2. All pressure distributions are calculated for the instant  $\hat{t} = 360$  s. It can be seen that decrease of pressure in the mushy

zone which follows from the analytical solution (36) exceeds decrease of pressure which follows from the numerical solution. This is because the analytical solution is obtained assuming that porosity formation does not influence the pressure distribution in the mushy zone. In fact, formation of porosity partly compensates the metal shrinkage. This leads to decrease of interdendritic fluid flow which compensates this shrinkage and, consequently, to a lesser pressure drop in the mushy zone.

The larger the pressure drop in the mushy zone, the larger the deviation between the analytical and the steady-state pressure distributions. This is because for larger pressure drop more porosity forms in the casting, thus there is a more significant influence of porosity formation on the pressure distribution. As expected, pressure drop increases with decrease of the dendrite size cell.

Comparison of residual porosity distributions calculated according to equation (37) utilizing analytical solution for pressure distribution (36) and the steady-state numerical solution for different values of dendrite cell size is depicted in Fig. 3. All porosity distributions are computed for duration of two-phase solidification  $\hat{t} = 360$  s. It can be seen that volume % of residual porosity calculated utilizing the analytical pressure distribution (36) is higher than that utilizing the steady-state numerical distribution. This is because pressure drop in the mushy zone according to analytical pressure distribution is overpredicted according to the steady-state numerical distribution as discussed in connection to Fig. 2. As expected from

physical considerations, the residual porosity increases with a decrease of the dendrite size cell.

3.3. Estimation of the error introduced by the quasi-stationary solution of porosity formation problem

The influence of the non-stationary term which was neglected in equation (27) can be estimated by the following function

$$\Delta(x, t) = \frac{\left| \frac{1}{2P^{1/2}} \frac{\partial P}{\partial t} S(f_s, T) [1 - f_s(1 - k_H)] \right|}{\left| \frac{\partial S(f_s, T)}{\partial t} P^{1/2} [1 - f_s(1 - k_H)] - S(f_s, T) P^{1/2} (1 - k_H) \frac{\partial f_s}{\partial t} \right|} \quad (39)$$

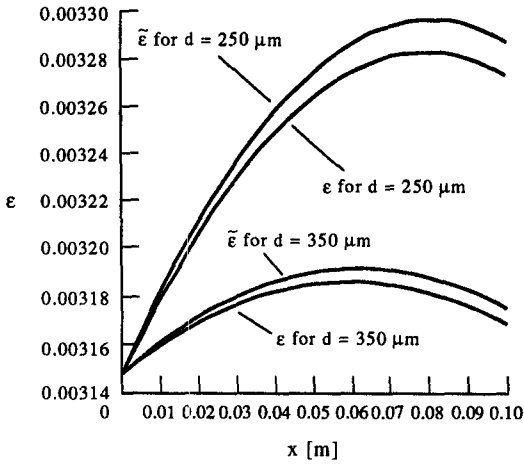


Fig. 3. Comparison of residual porosity distributions calculated according to equation (37) utilizing analytical solution for pressure distribution (36) and the steady-state numerical solution for different values of dendrite cell size:  $\tilde{\varepsilon}$ , analytical;  $\varepsilon$ , steady-state numerical.

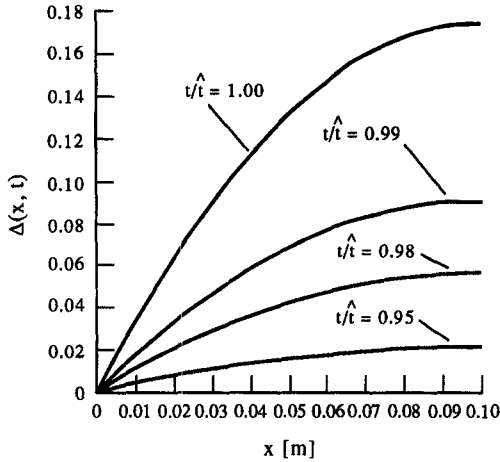


Fig. 4. Influence of non-stationary pressure term in equation (27) calculated for different values of the ratio  $t/\hat{t}$ .

The function  $\Delta(x, t)$  shows the influence of the non-stationary part of the second term in equation (27). The derivative  $\partial P/\partial t$  in equation (39) can be estimated from equation (36).

Figure 4 depicts the dependence  $\Delta(x)$  for different values of the ratio  $t/\hat{t}$ , where  $\hat{t}$  signifies the time that it takes to reach the eutectic temperature. Calculations are carried out for duration of two-phase solidification  $\hat{t} = 360$  s and dendrite cell size  $d = 350$   $\mu\text{m}$ . As it follows from the figure, the steady-state approximation introduces maximum error at the end of the two-phase solidification process. This is because maximum decrease of pressure in the mushy zone is when the amount of liquid phase is minimum, that is at the end of two-phase solidification. Therefore influence of non-stationary part on the second term in equation (27) is maximum at the end of two-phase solidification. It can be seen that the maximum error

introduced by neglecting the non-stationary part in the second term is about 17%. The error quickly decreases with decrease of the ratio  $t/\hat{t}$ .

### 3.4. Analytical criterion for the absence of porosity in the casting process

From equation (37) it follows that no porosity arises at the end of the first stage of solidification if

$$\theta(C_{H0} - K_0 S(1 - f_E, T_E) P^{1/2} [1 - (1 - f_E)(1 - k_H)]) = 0. \quad (40)$$

Equation (40) is satisfied if

$$C_{H0} - K_0 S(1 - f_E, T_E) P_{\min}^{1/2} [1 - (1 - f_E)(1 - k_H)] \leq 0 \quad (41)$$

where  $P_{\min}$  is the minimum pressure in the casting at  $t = \hat{t}$ . Because we are interested in the case when no porosity forms in the casting, equation (36) can determine the pressure distribution in the casting. Using equation (36), the location for minimum pressure,  $\bar{x}$ , in the casting process can be determined from the following equation

$$\left. \frac{\partial P}{\partial x} \right|_{x=\bar{x}} = \rho_L g - \beta \frac{5\mu M_S^2 f_S^2}{(1 - f_S)^3} \left. \frac{\partial f_S}{\partial t} \right|_{t=\hat{t}} (L - \bar{x}) = 0 \quad (42)$$

where according to equation (35)

$$\left. \frac{\partial f_S}{\partial t} \right|_{t=\hat{t}} = (1 - f_E) \Omega \frac{T_L - T_{\text{ch}}}{T_L - T_E} \exp(-\Omega \hat{t}).$$

From equation (42) it follows that

$$\bar{x} = L - \frac{\rho_L g}{\Lambda(\hat{t})} \quad (43)$$

where

$$\Lambda(\hat{t}) = \beta \frac{5\mu M_S^2 (1 - f_E)^3}{f_E^3} \Omega \frac{T_L - T_{\text{ch}}}{T_L - T_E} \exp(-\Omega \hat{t}).$$

Equation (43) is valid while  $L - (\rho_L g / \Lambda(\hat{t})) \geq 0$ . When the value of  $L - (\rho_L g / \Lambda(\hat{t}))$  becomes negative, the position of pressure minimum in the casting is  $\bar{x} = 0$ . Finally, the coordinate of pressure minimum in the casting is determined by the following equation

$$\bar{x} = \left[ L - \frac{\rho_L g}{\Lambda(\hat{t})} \right] \theta \left[ L - \frac{\rho_L g}{\Lambda(\hat{t})} \right]. \quad (44)$$

From equations (36) and (44) it follows that

$$P_{\min} = P_{\text{atm}} + \left\{ \rho_L g \left[ L - \frac{\rho_L g}{\Lambda(\hat{t})} \right] - \Lambda(\hat{t}) \left[ L - \frac{\rho_L g}{\Lambda(\hat{t})} \right] \left( \frac{L}{2} + \frac{\rho_L g}{2\Lambda(\hat{t})} \right) \right\} \theta \left[ L - \frac{\rho_L g}{\Lambda(\hat{t})} \right]. \quad (45)$$

From equations (41) and (45) it follows that no porosity arises in the casting if

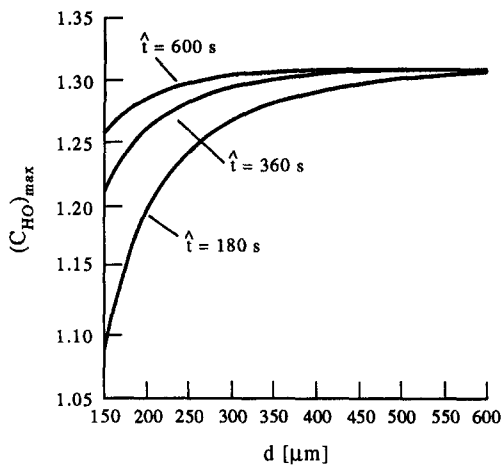


Fig. 5. Dependence of the maximum initial hydrogen concentration  $(C_{H0})_{max}$  in the alloy on the size of dendrite cell  $d$  for different duration of two-phase solidification  $\hat{t}$  so that porosity does not arise.

$$C_{H0} - K_0 S(1 - f_E, T_E) [1 - (1 - f_E)(1 - k_H)] \times \left\{ P_{atm} + \left\{ \rho_L g \left[ L - \frac{\rho_L g}{\Lambda(\hat{t})} \right] - \Lambda(\hat{t}) \left[ L - \frac{\rho_L g}{\Lambda(\hat{t})} \right] \left( \frac{L}{2} + \frac{\rho_L g}{2\Lambda(\hat{t})} \right) \right\} \theta \left[ L - \frac{\rho_L g}{\Lambda(\hat{t})} \right]^{1/2} \right\} \leq 0. \quad (46)$$

Equation (46) gives the analytical criterion of absence of porosity in the casting.

Figure 5 depicts dependence of the maximum initial hydrogen concentration  $(C_{H0})_{max}$  in the alloy on the size of dendrite cell  $d$  for different duration of two-phase solidification  $\hat{t}$  so that porosity does not arise. It can be seen that  $(C_{H0})_{max}$  increases with an increase of the dendrite cell size until it reaches some constant value. This constant value also does not depend on duration of two-phase solidification and corresponds to the situation when  $P(x, \hat{t}) \approx P_{atm}$ . Until this constant value is reached,  $(C_{H0})_{max}$  is larger for larger values of  $\hat{t}$ . This is because the larger the duration of two-phase solidification, the less interdendritic fluid flow is required to compensate metal shrinkage, a lesser pressure drop is required in the mushy zone and, consequently, the maximum initial hydrogen concentration has to be larger so that porosity does not arise.

#### 4. CONCLUSIONS

In this work the three-phase model (liquid, solid and gas) of the mushy zone is suggested. Using this model, influence of porosity formation on pressure and residual porosity distributions in the mushy zone is investigated. For this investigation thermodynamic relationships for the particular case of Al-rich Al-Cu alloys are utilized. It is shown that the porosity formation leads to less pressure drop and an underprediction of the residual porosity. The influence

porosity formation increases with an increase in the pressure drop.

It is also shown that for no porosity formation the maximum initial hydrogen concentration in the alloy has to increase with an increase of the dendrite cell size until it reaches some constant value. This constant value does not depend on duration of the two-phase solidification and corresponds to the situation when pressure in the mushy zone at the end of two-phase solidification approximately equals the atmospheric pressure.

Analysis carried out in this work establishes useful and practical criterion for absence of porosity in casting during uniform solidification.

*Acknowledgement*—One of the authors (A.V.K.) is grateful to AvHumboldt Foundation (Germany) for a research fellowship which gave possibility to obtain some of the results presented in this paper. His Ohio State University Postdoctoral Fellowship is also gratefully acknowledged and appreciated.

#### REFERENCES

1. T. S. Piwonka and M. C. Flemings, Pore formation in solidification, *AMS-AIME Trans.* **236**, 1157–1165 (1966).
2. V. de L. Devies, Feeding range determination by numerically computed heat distribution, *AFS Cast Metals Res. J.* **11**, 33–44 (1975).
3. E. Niyama, T. Uchida, M. Morikawa and S. Saito, A method of shrinkage prediction and its application to steel casting practice, *AFC Cast Metals Res. J.* **7**, 52–63 (1982).
4. E. N. Pan, C. S. Lin and C. R. Loper, Effects of solidification parameters on the feeding efficiency of A356 aluminum alloy, *AFC Trans.* **98** (1990).
5. P. N. Hansen and J. T. Berry, The simulation of heat transfer in castings and weldments—some thoughts of needed research. In *Modeling of Casting and Welding Process*, pp. 497–501 (1981).
6. S. Viswanathan, V. K. Sikka and H. D. Brody, Using solidification parameters to predict porosity distribution in alloy castings, *JOM* **44**, 37–40 (1992).
7. H. Huang, V. K. Suri, and J. L. Hill, Issues in thermal contact and phase change in porosity prediction, *ASME J. Engng Mater. Technol.* **115**, 2–7 (1993).
8. J. Lecomte-Beckers, Study of microporosity formation in nickel-base superalloys, *Metall. Trans.* **19A**, 2341–2348 (1988).
9. Y. W. Lee, E. Chang and C. F. Chieu, Modeling of feeding behavior of solidifying Al-7Si-0.3Mg alloy plate casting, *Metall. Trans.* **21B**, 715–722 (1990).
10. Ph. Thevoz, J. L. Desbiolles and M. Rappaz, Modeling of equiaxed microstructure formation in casting, *Metall. Trans.* **20A**, 311–322 (1989).
11. D. M. Stefanescu, G. Upadhyaya and D. Bandyopadhyay, Heat transfer-solidification kinetics modeling of solidification of castings, *Metall. Trans.* **21A**, 997–1005 (1990).
12. K. Kubo and R. D. Pehlke, Mathematical modeling of porosity formation in solidification, *Metall. Trans.* **16B**, 359–366 (1985).
13. D. R. Poirier, K. Yeum and A. L. Maples, A thermodynamic prediction for microporosity formation in aluminum-rich Al-Cu alloys, *Metall. Trans.* **18A**, 1979–1987 (1987).
14. W. D. Bennon and F. P. Incropera, A continuum model for momentum, heat and species transport in binary

- solid-liquid phase change systems—I. Model formulation, *Int. J. Heat Mass Transfer* **30**, 2161–2170 (1987).
15. P. J. Prescott, F. P. Incropera and W. D. Bennon, Modeling of dendritic solidification systems: reassessment of the continuum momentum equation, *Int. J. Heat Mass Transfer* **34**, 2351–2359 (1990).
  16. S. Ganesan and D. R. Poirier, Conservation of mass and momentum for the flow of interdendritic liquid during solidification, *Metall. Trans.* **21B**, 173–181 (1990).
  17. J. Ni and C. Beckermann, A volume-averaged two-phase model for transport phenomena during solidification, *Metall. Trans.* **22B**, 349–361 (1991).
  18. C. Beckermann and R. Viskanta, Double-diffusive convection during dendritic solidification of a binary mixture, *PhysicoChem. Hydrodyn.* **10**, 195–213 (1988).
  19. S. D. Felicelli, J. C. Heinrich and D. R. Poirier, Simulation of freckles during vertical solidification of binary alloys, *Metall. Trans.* **22B**, 847–859 (1991).
  20. S. D. Felicelli, J. C. Heinrich and D. R. Poirier, Numerical model for dendritic solidification of binary alloys, *Numer. Heat Transfer* **B23**, 461–481 (1993).
  21. R. Mehrabian, M. Keane and M. C. Flemings, Interdendritic fluid flow and macrosegregation: influence of gravity, *Metall. Trans.* **1**, 1209–1220 (1970).
  22. N. Streat and F. Weinberg, Macrosegregation during solidification resulting from density differences in the liquid, *Metall. Trans.* **5**, 2539–2548 (1974).
  23. T. Fujii, D. R. Poirier and M. C. Flemings, Macrosegregation in a multi-component low alloy steel, *Metall. Trans.* **10B**, 331–339 (1979).
  24. S. D. Ridder, S. Kou and R. Mehrabian, Effect of fluid flow on macrosegregation in axi-symmetric ingots, *Metall. Trans.* **12B**, 435–447 (1981).
  25. A. L. Maples and D. R. Poirier, Convection in the two-phase zone of solidifying alloys, *Metall. Trans.* **15B**, 163–172 (1984).
  26. D. R. Poirier, Permeability for flow of interdendritic liquid in columnar-dendritic alloys, *Metall. Trans.* **18B**, 245–255 (1987).
  27. J. Ampuero, A. F. A. Hoadley and M. Rappaz, Numerical and experimental study of microporosity evolution during the solidification of metallic alloys. In *Modeling of Casting, Welding and Advanced Solidification Processes*, Vol. 5, pp. 449–454 (1991).
  28. W. R. Opie and N. J. Grant, *Trans. AIME, J. Metals* **188**, 1237–1241 (1950).
  29. M. Rappaz and V. Voller, Modeling of micro-macro-segregation in solidification processes, *Metall. Trans.* **21A**, 749–753 (1990).
  30. M. A. Taha, N. A. El-Mahallawy, A. W. M. Assar and R. M. Hammouda, Effect of melt superheat and chill material on interfacial heat-transfer coefficient in end-chill Al and Al–Cu alloy castings, *J. Mater. Sci.* **27**, 3467–3473 (1992).
  31. H. Huang, J. L. Hill and J. T. Berry, A free thermal contraction method for modeling the heat-transfer coefficient at the casting–mold interface, *Cast Metals* **5**, 212–216 (1993).
  32. J. T. Berry, The role of the mold–metal interface in net shape aluminum castings. In *Casting of Near Net Shape Products*, pp. 41–50. TMS (1988).
  33. J. L. Murray, The aluminum–copper system, *Int. Metals Rev.* **30**, 211–233 (1985).
  34. K. Vafai and C. L. Tien, Boundary and inertia effects on convective mass transfer in porous media, *Int. J. Heat Mass Transfer* **25**(1), 1183–1190 (1982).
  35. K. Vafai, Convective flow and heat transfer in variable-porosity media, *J. Fluid Mech.* **147**, 233–259 (1984).
  36. K. Vafai, Analysis of the channeling effect in variable porosity media, *J. Energy Resour. Technol.* **108**, 131–139 (1986).
  37. A. Amiri and K. Vafai, Analysis of dispersion effects and non-thermal equilibrium non-darcian, variable porosity incompressible flow through porous medium, *Int. J. Heat Mass Transfer* **37**, 939–954 (1994).
  38. K. Vafai and M. Sözen, Analysis of energy and momentum transport for fluid flow through a porous bed, *J. Heat Transfer* **112**, 690–699 (1990).
  39. M. Sözen and K. Vafai, Longitudinal heat dispersion in porous beds with real gas flow, *J. Thermophys. Heat Transfer* **7**(1), 153–157 (1993).